JOURNAL OF GEOPHYSICAL RESEARCH: SOLID EARTH, VOL. 118, 2371–2381, doi:10.1002/jgrb.50154, 2013

A decade of horizontal deformation from great earthquakes

P. Tregoning,[1] R. Burgette,[2,4] S. C. McClusky,[1] S. Lejeune,[3] C. S. Watson,[2] and H. McQueen[1]

Received 11 September 2012; revised 13 February 2013; accepted 10 March 2013; published 6 May 2013.

[1] The 21st Century has seen the occurrence of 17 great earthquakes (Mw>8), including some of the largest earthquakes ever recorded. Numerical modeling of the earthquakes shows that nearly half of the Earth's surface has undergone horizontal coseismic deformation >1 mm, with the 2004 Sumatra-Andaman earthquake dominating the global deformation field. This has important implications for both the realization of a terrestrial reference frame and in the interpretation of regional tectonic studies based on GPS velocities. We show that far-field coseismic deformations from great earthquakes will, if unaccounted for, introduce errors in estimates of linear site velocities of at least 0.1-0.3 mm/yr across most of the surface of the Earth. The accumulated global deformation field shows that two regions, Australia and the north Atlantic/Arctic Ocean, have been largely undeformed by these great earthquakes, with accumulated deformations generally <0.5 mm. Using GPS estimates of surface deformation, we show that the majority of the Australian continent is deforming at <0.2 mm/yr, the northern part of New Zealand is rotating clockwise relative to the Australian Plate with relative horizontal velocities of ∼2 mm/yr, while the southeastern coast of Australia is undergoing post-seismic relaxation caused by the 2004 Mw = 8.1 Macquarie Ridge earthquake. The presence of ongoing post-seismic relaxation thousands of kilometers from plate margins violates the secular/linear assumption made in current terrestrial reference frame definitions. These effects have significant ramifications for regional tectonic interpretations and global studies such as sea level rise that require reference frame accuracy greater than this level.

Citation: Tregoning, P., R. Burgette, S. C. McClusky, S. Lejeune, C. S. Watson, and H. McQueen (2013), A decade of horizontal deformation from great earthquakes, *J. Geophys. Res. Solid Earth*, *118*, 2371–2381, doi:10.1002/jgrb.50154.

1. Introduction

[2] Strain accumulation and release within the Earth's tectonic plates occur over a wide range of spatial and temporal and scales throughout the seismic cycle. Conventional plate tectonic theory is built around the premise that the plates are rigid, an assumption that underpins the coordinate reference frames relied upon by Earth-observing space missions for measuring the dynamic Earth system [e.g., *Altamimi et al.*, 2012]. Today's modern space geodetic techniques enable the determination with unprecedented precision of where, when and at what rate tectonic plates are deforming.

[3] Whether tectonic plates behave as rigid bodies has ramifications for how the surface of the Earth evolves over time. The coordinate reference frame used on Earth underpins many scientific studies (e.g., sea level rise, crustal deformation, satellite orbit estimation, etc.), and its accuracy relies upon representing correctly the temporal movement of the tracking stations on Earth. The assumption that tectonic plates move as rigid bodies implies that site velocities will be linear on short time scales, and to what extent this assumption is correct directly affects our ability to construct accurately a temporally varying reference frame. It is timely to readdress the question of the rigidity of tectonic plates in light of the occurrence of great megathrust earthquakes that have deformed the Earth over many thousands of kilometers [e.g., *Kreemer et al.*, 2006]. What upper bound can be placed on the rigidity of large tectonic elements, particularly those regions that are distant from great earthquakes, and how do assumptions of large-scale plate rigidity affect regional tectonic studies?

[4] Detection of far-field coseismic displacements greater than a few millimeters caused by the Sumatra-Andaman earthquake [e.g., *Vigny et al.*, 2005; *Fu and Sun*,

Additional supporting information may be found in the online version of this article.

[1]Research School of Earth Sciences, The Australian National University, Canberra, ACT, Australia.
[2]Surveying and Spatial Science Group, School of Geography and Environmental Studies, University of Tasmania, Hobart, Tasmania, Australia.
[3]Royal Meteorological Institute of Belgium, Brussels, Belgium.
[4]Now at Department of Geological Sciences, University of Oregon, Eugene, Oregon, USA.

Corresponding author: P. Tregoning, Research School of Earth Sciences, The Australian National University, Canberra, ACT, Australia. (paul.tregoning@anu.edu.au)

2169-9313/13/10.1002/jgrb.50154

Table 1. Great Earthquakes Whose Coseismic Horizontal Deformation Is Modeled in This Study

#	Earthquake	Date	Magnitude	Source
1	New Ireland, PNG	16 Nov 2000	8.0	*Park and Mori* [2007]
2	South Peru	23 Jun 2001	8.4	*Pritchard et al.* [2007]
3	Hokkaido, Japan	25 Sep 2003	8.3	*Romano et al.* [2010]
4	Macquarie Island	23 Dec 2004	8.1	*Watson et al.* [2010]
5	Sumatra-Andaman	26 Dec 2004	9.3	*Banerjee et al.* [2007]
6	Northern Sumatra	28 Mar 2005	8.6	*Banerjee et al.* [2007]
7	Tonga	03 May 2006	8.0	*Ekström et al.* [2012]
8	Kuril Islands	25 Nov 2006	8.3	*Lay et al.* [2009]; *Ekström et al.* [2012]
9	East of Kuril Islands	13 Jan 2007	8.1	*Lay et al.* [2009]; *Ekström et al.* [2012]
10	Solomon Islands	01 Apr 2007	8.1	*Furlong et al.* [2009]
11	Central Peru	15 Aug 2007	8.0	*Sladen et al.* [2010]
12	Southern Sumatra	12 Sep 2007	8.5	*Konca et al.* [2008]
13	Samoa	29 Sep 2009	8.1	*Lay et al.* [2010]; *Beavan et al.* [2010]
14	Maule, Chile	27 Feb 2010	8.8	*Lorito et al.* [2011]
15	Tohoku-Oki, Japan	11 Mar 2011	9.1	*Simons et al.* [2011]

2006; *Kreemer et al.*, 2006] show the power of using Global Positioning System (GPS) estimates to quantify global deformation, although very distant (i.e., > 1000 km) displacements caused by the smaller of the great earthquakes have not previously been identified. Recent improvements in the analysis of GPS observations [e.g., *Boehm et al.*, 2006] have provided the ability to detect temporal variations in site movements at the submillimeter level [e.g., *Steigenberger et al.*, 2009; *Tregoning and Watson*, 2009, 2011], and to make velocity estimates with a precision of 0.3 mm/yr [*Altamimi et al.*, 2012]. This improvement offers the potential to identify regions where the crust is more stable than these detection levels and, importantly, the ability to detect very far-field coseismic displacements and post-seismic deformation.

[5] In this study, we calculate the global pattern of coseismic deformation from 15 earthquakes $M_w > 8$ since 2000 using a spherical elastic dislocation model. Modeled far-field deformations are of comparable size and typically small (i.e., < 1–2 mm) in both horizontal and vertical components. For the vertical deformations, this level of deformation is well below the inherent noise levels in current GPS analyses, caused by noise introduced through the mismodeling of tropospheric effects [e.g., *Steigenberger et al.*, 2009; *Tregoning and Watson*, 2009], ocean tide and non-tidal ocean loading effects [e.g., *Williams and Penna*, 2011] and spurious periodic signals that have aliased through the estimation process to harmonics of the GPS draconitic year (351.4 days) [e.g., *Ray et al.*, 2008; *Tregoning and Watson*, 2009]. As a result, not accounting for vertical coseismic deformations at far-field sites will have an undetectable effect on the reference frame used in GPS analysis at the present time. We therefore limit our analysis to the horizontal components where the deformation is detectable, and hence must be considered.

[6] We use the Australian Plate as a case study to demonstrate how the realization of the coordinate reference frame in the GPS analysis can lead to different tectonic interpretations, and show that significant crustal deformation effects occurring thousands of kilometers from plate boundary zones might be overlooked unless far-field horizontal deformation from great earthquakes are taken into consideration. Focusing on the Australiasian region, we compare our modeled coseismic horizontal deformations with those estimated from time series of positions derived from a decade of global GPS data. Finally, after accounting for non-tectonic (instrumental) offsets in the time series, we assess the level of rigidity and physical extent of the rigid Australian Plate.

2. Earthquake Modeling

[7] We derived model estimates of static coseismic deformation using a spherical layered model [*Pollitz*, 1996]. Surface deformation is calculated assuming the PREM elastic stratification [*Dziewonski and Anderson*, 1981], with a spherical harmonic expansion from degrees 1 to 1500. Below, we describe the modeling of 15 earthquakes of $M_w > 8$ (Table 1) that have occurred since 2000 [*Ekström et al.*, 2012]. These calculations assume a static Earth, and our investigation focuses on the horizontal distortion of the Earth's surface by great earthquakes. We use a variety of rupture and slip distribution models, prioritizing published results that explicitly specify the spatial extent of slip on fault planes. For events that lack published slip distribution information in tabular form, we generalized fault planes with uniform slip over an area approximately coincident with that estimated from published teleseismic investigations, and a magnitude of slip consistent with the moment magnitude estimated in the seismic investigation(s) (for far-field deformation, the actual details of the slip distribution are much less important than for modeling near-field deformation, and we found < 0.5 mm differences in modeled far-field coseismic deformations when using different rupture and slip distribution models). Fault parameters for which we have assumed a uniform slip model are provided in the supporting information (Table S1).

2.1. Great Earthquakes

2.1.1. 2000 Papua New Guinea

[8] We model the 16 November 2000 Mw 8.0 New Ireland area earthquake as left-oblique reverse slip on the Weitin Fault, with the geometry and rake of the rupture from a seismic study [*Park and Mori*, 2007]. We constrain the moment to the value from the Global Centroid Moment Tensor project (GCMT) [*Ekström et al.*, 2012], which is intermediate among the reported estimates [*Park and Mori*, 2007].

2.1.2. 2001 Peru

[9] We model the 23 June 2001 Mw 8.5 Arequipa, Peru earthquake with uniform slip on a single plane coincident with the area of the majority of the slip as inferred by a joint seismic and geodetic study [*Pritchard et al.*, 2007]. The rake and moment are mean values [*Pritchard et al.*, 2007].

2.1.3. 2003 Japan

[10] The 25 September 2003 Mw 8.1 Tokachi-Oki earthquake occurred along the southwestern Kuril Trench. We model the earthquake using a slip distribution constrained by GPS and tsunami observations [*Romano et al.*, 2010].

2.1.4. 2004 Macquarie Ridge

[11] The 23 December 2004 Mw 8.2 earthquake occurred as strike-slip on a fracture zone west of Macquarie Ridge in the Australian plate. We use a previously published fault geometry derived from seismic locations and regional GPS observations [*Watson et al.*, 2010], with an updated inversion for slip using Greens functions calculated with the spherical layered elastic model [*Pollitz*, 1996]. The mean horizontal velocity residual is reduced to 1.2 mm/yr, and the estimated moment is approximately double that inferred from a non-spherical homogeneous elastic half-space [*Watson et al.*, 2010].

2.1.5. 2004 Sumatra-Andaman

[12] The 26 December 2004 Mw 9.2 earthquake ruptured the northern Sumatra and Andaman portions of the Indo-Australian-Eurasia plate boundary. We use a static slip distribution [*Banerjee et al.*, 2007] (model C) derived from regional GPS displacements and the spherical layered deformation code [*Pollitz*, 1996] used here.

2.1.6. 2005 Sumatra

[13] The 28 March 2005 Mw 8.7 Nias earthquake ruptured the northern Sumatra megathrust immediately south of the 2004 great earthquake. We again use the slip distribution from a geodetic study [*Banerjee et al.*, 2007].

2.1.7. 2006 Tonga

[14] The 5 May 2006 Mw 8.0 earthquake occurred along the Tonga subduction zone. We model the earthquake using a single plane with uniform slip. The geometry and extent are constrained by plate boundary orientation, GCMT [*Ekström et al.*, 2012] parameters and aftershocks. We use GCMT estimates to constrain the moment and slip direction. Our source model is similar to that used in a tsunami study [*Tang et al.*, 2008].

2.1.8. 2006 Kuril Islands

[15] The 15 November 2006 Mw 8.3 thrust earthquake ruptured a portion of the Kuril subduction fault. We model this earthquake with a uniform slip, planar fault approximately coincident with the area of > 1 m slip reported in a seismic investigation [*Lay et al.*, 2009]. The mean slip orientation is taken from this seismic study, and we constrain the slip magnitude such that the moment is equal to the GCMT solution [*Ekström et al.*, 2012]. The GCMT magnitude is intermediate amongst several estimates [*Lay et al.*, 2009].

2.1.9. 2007 Kuril Islands

[16] The 13 January 2007 Mw 8.1 earthquake occurred as normal faulting in the subducting Pacific Plate, immediately east of the 2006 rupture. As with the 2006 event, we model the deformation using a geometry and slip direction based on a finite fault seismic inversion [*Lay et al.*, 2009], and an intermediate estimate of moment from the GCMT [*Ekström et al.*, 2012].

2.1.10. 2007 Solomon Islands

[17] The 1 April 2007 Mw 8.1 Solomon Islands earthquake occurred as dominantly thrust slip along the Solomon Islands subduction zone across a triple junction. We model the earthquake assuming uniform slip with moment and average slip direction as inferred from seismic observations [*Furlong et al.*, 2009]. The extent of the rupture plane is constrained by aftershocks and the spatial extent of the slip from the seismic finite fault inversion.

2.1.11. 2007 Peru

[18] The 15 August 2007 Mw 8.0 Pisco, Peru earthquake ruptured a section of the South America-Nazca plate boundary north of the axis of the subducting Nazca ridge. We use a slip distribution jointly constrained with seismic and InSAR observations [*Sladen et al.*, 2010]. (downloaded from http://www.tectonics.caltech.edu/slip_history/2007_peru/pisco-update.html).

2.1.12. 2007 Sumatra

[19] The 12 September 2007 Mw 8.4 southern Sumatra earthquake ruptured a portion of the Sumatra megathrust farther to the southeast than the 2005 earthquake. We use a slip distribution constrained with seismic and geodetic observations [*Konca et al.*, 2008]. (downloaded from http://www.tectonics.caltech.edu/slip_history/2007_s_sumatra/ssumatra-update.html).

2.1.13. 2009 Samoa-Tonga

[20] The 29 September 2009 great earthquake doublet involved contemporaneous or nearly contemporaneous slip on both the Tonga subduction thrust interface and a normal fault in the subducting Pacific Plate, with each sub-event having a moment magnitude of 8.0 [*Lay et al.*, 2010; *Beavan et al.*, 2010]. Here, we use the two fault source model inferred from GPS and tsunami observations [*Beavan et al.*, 2010].

2.1.14. 2010 Chile

[21] The 27 February 2010 Mw 8.8 megathrust earthquake ruptured the South America-Nazca plate boundary in the Maule, Chile region. We use a slip distribution constrained by geodetic and tsunami data [*Lorito et al.*, 2011].

2.1.15. 2011 Japan

[22] The 11 March 2011 Mw 9.0 Tohoku-Oki thrust earthquake ruptured a portion of the Pacific-Okhotsk plate boundary. We use a static slip distribution constrained by GPS and tsunami observations [*Simons et al.*, 2011]. In our model, the complex triangular sub-fault geometry is approximated with 227 rectangular subfaults that include one along-strike change in the strike direction, and a change in dip with depth that is averaged along-strike. We resample the published slip distribution to our geometry such that the spatial distribution of slip magnitude and azimuth are preserved.

2.2. Accumulated Deformation

[23] The accumulated modeled coseismic horizontal deformation caused by these events exceeds 1 mm over much of the Earth (Figure 1) and is dominated by the contribution of the Sumatra-Andaman earthquake, with lobes of deformation spreading NE and SW from the megathrust boundary. We calculate coseismic horizontal displacements as far afield as Flin Flon in central Canada

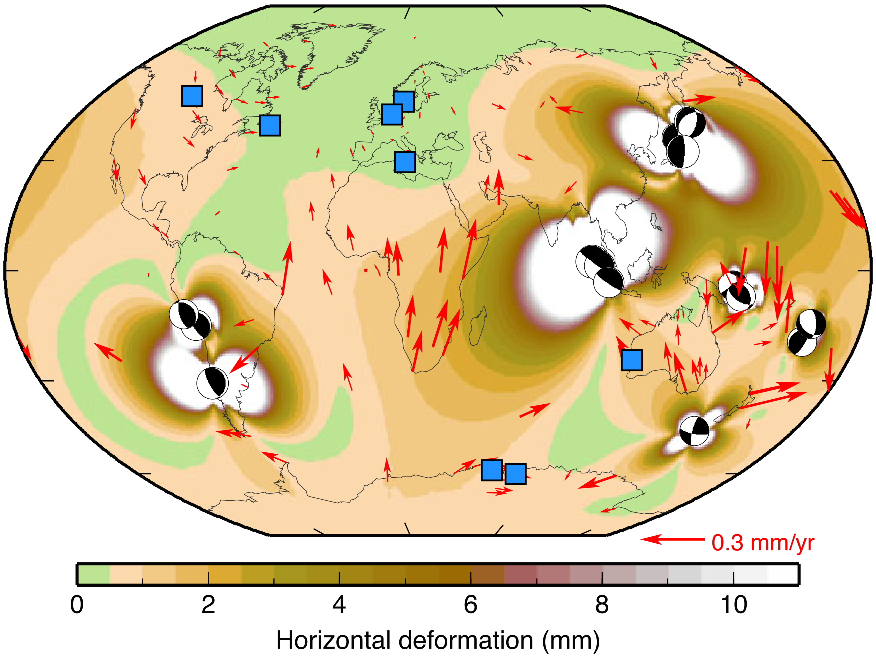

Figure 1. Accumulated coseismic horizontal deformation field of great earthquakes (M_w > 8) since 2000. Focal mechanisms are from the Global Moment Tensor catalog [*Ekström et al.*, 2012]. GPS sites used to define the terrestrial reference frame are shown (blue squares), along with far-field site velocity errors (red arrows) induced by not accounting for the coseismic horizontal deformations of the great earthquakes.

(0.7 mm), 1.5 mm at Capetown, South Africa and 0.5 mm in Santiago, Chile. This is in general agreement with the computations of, for example, *Fu and Sun* [2006], but is notably smaller in magnitude across Africa and South America than the results of *Kreemer et al.* [2006] (the spherical layer model code of *Pollitz* [1996] used in their study did not accurately calculate deformation over the longest spatial scales. The version of the code used in this study is appropriate for full global calculations (F. Pollitz, personal communication, July 2011)). Modeling shows that the regions in the direction of the prolongation of the strike of the thrust (i.e., NW across Europe and SE across Australia) experienced much smaller coseismic horizontal deformations, with magnitudes < 0.5 mm (Figure 2a).

[24] In contrast, the February 2011 Tohoku-Oki earthquake caused smaller far-field coseismic horizontal deformations because a significant part of the energy release occurred at depths greater than 30 km [e.g., *Yagi and Fukahata*, 2011], thus reducing the magnitude of the induced surface deformations. The energy release was also smaller than the Sumatra-Andaman earthquake [*Ekström et al.*, 2012]. The lobes of major deformation extend to the east (into the Pacific) and west of Japan, affecting eastern Europe, but again essentially missing the Australian region (Figure 2b). The other earthquakes with magnitudes $8 < M_w < 9$ caused coseismic horizontal displacements of several meters in the near-field regions but, at distances > 1000–2000 km, the displacement field

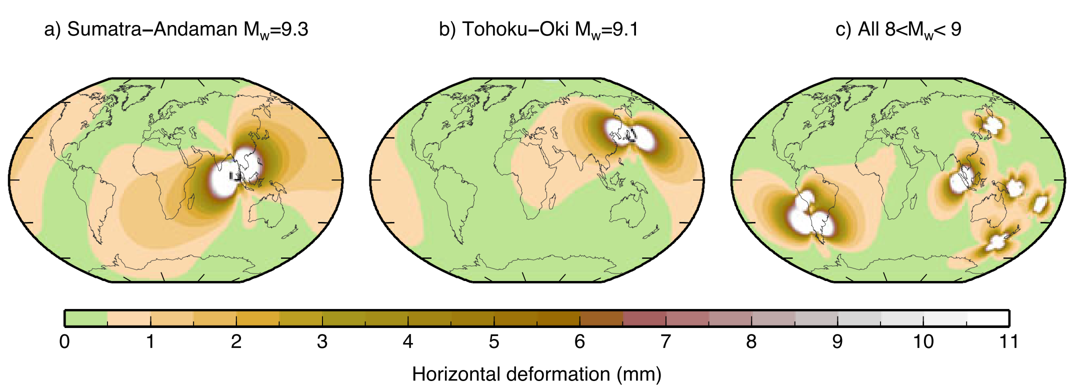

Figure 2. Magnitude of coseismic horizontal deformation of the (a) Sumatra-Andaman, (b) Tohoku-Oki earthquakes and (c) the sum of all other great earthquakes since 2000.

reduces to < 1 mm. Thus, viewed from a global perspective, these earthquakes have a more minor effect on the total deformation of the Earth (Figure 2c). The Australian continent, western Europe and the eastern tip of Canada are the only sub-aerial regions with an average coseismic horizontal deformation less than 0.5 mm (Figure 1).

[25] We find that the magnitude of slip required to explain the observed deformation pattern of the 2004 Macquarie Ridge earthquake is 80% greater than previously reported [*Watson et al.*, 2010]; however, the model in that study was a flat-Earth, layered model whereas we use here a spherical, homogeneous half-space elastic dislocation model [*Pollitz*, 1996]. Our new model predicts deformation of up to 1 mm further north and northwest into the Australian continent (see Figure 2c); however, we do not detect these deformations in our GPS time series. This discrepancy is similar to tests presented by *Banerjee et al.* [2007], who attributed the differences to the consequences of layered elastic properties and sphericity assumptions, where the latter reduces the discrepancy with greater distance.

3. Data Analysis

3.1. GPS Analysis and Reference Frame Definition

[26] Our GPS analysis of over 100 global sites was performed with the GAMIT software [*Herring et al.*, 2010], employing time-varying modeling of atmospheric delays, mapping functions and atmospheric pressure loading deformation [*Tregoning and Watson*, 2009, 2011]. We aligned our daily, global GPS solutions from 2000 to 2011.0 with the International Terrestrial Reference Frame 2008 [*Altamimi et al.*, 2011] by computing six-parameter transformations (three-rotations, three-translations) of coordinates of eight reference sites (Figure 1 and described below). A significant coseismic displacement (~0.7 mm) at the time of the Sumatra-Andaman earthquake was detected and removed at site Flin Flon (FLIN); otherwise, no significant earthquake deformations were apparent at these reference sites.

3.2. Reference Frame Definition

[27] A fundamental reference frame is defined by an origin, three orthogonal axes and scale [*Altamimi et al.*, 2011]. For the International Terrestrial Reference Frame (ITRF), the origin is defined from the analysis of Satellite Laser Ranging (SLR) measurements to satellites orbiting the center of mass of the Earth such that there are zero translations and rotation rates with respect to the center of mass of the Earth, while the scale is defined from the mean of scale estimates from SLR and Very Long Baseline Interferometry (VLBI) long-term solutions [*Altamimi et al.*, 2011]. The realization of the terrestrial reference frame—and the way that users of the frame can access the information—is through the use of the coordinates of sites located on the surface of the Earth.

[28] The fact that much of the Earth is affected by coseismic deformation from these great earthquakes is problematic for the definition of the terrestrial reference frame that is used to underpin all geophysical studies using space geodetic techniques. Because the coseismic displacement field caused by each earthquake occurs over a matter of seconds to minutes (GPS solutions are typically averaged to daily or weekly values), it becomes difficult to estimate the offsets at individual sites, particularly when many sites may have been displaced simultaneously. What then is the effect of unmodeled coseismic displacements on the definition of the reference frame? Earthquakes have a strong tendency to deform the shape of the Earth towards being less oblate [*Chao and Gross*, 1987]; one should question to what extent the center of mass of the Earth changes as a result of any earthquake, but great earthquakes in particular, since the deformation pattern can cover much of the Earth.

[29] If the center of mass of the Earth were to move with respect to the surface of the Earth because of coseismic deformation, then the entire set of coordinates required to define the ITRF would have to change because the pre- and post-earthquake vectors between a site on the surface and the origin would be different. Even the coordinates of a site located in a region that did not undergo far-field deformation would be different before and after an earthquake if the origin of the coordinate system changed location.

[30] *Gross and Chao* [2006] assessed the effect of the 2004 Sumatra-Andaman earthquake on the rotation and the gravity field of the Earth. They computed that the length-of-day would have decreased by 6.8 ms, the pole of rotation would have moved by 2.32 mas and that the Earth's oblateness would have reduced by 2.37×10^{-11}. They concluded that the rotational effects were smaller (by a factor of ~3) than the current observational accuracy, but that the change in oblateness should be detectable. Importantly, their study made the assumption that the origin of the coordinate system was at the center of mass of the Earth (i.e., that the degree 1 terms of the change in gravitational potential were zero); that is, that the origin did not move as a result of the earthquake. Thus, no consideration was given to the problem articulated above concerning earthquake induced movement of the center of mass of the Earth relative to the surface.

[31] Because it is predominantly the surface shell that deforms in a shallow megathrust event, we computed the change in center of mass of a 10 m thick shell at the surface of the Earth (assuming a spherical Earth) for the modeled coseismic deformations of the Sumatra-Andaman earthquake, the largest recorded great earthquake. The translation of the origin induced by the deformation was 0.3, 0.9 and –1.3 mm for the X, Y and Z components, respectively (we used a mean density of 3000 kg/m^3 in our computations). However, when the interior of the Earth is added to the computation, these values decrease to < 3 nm. Thus, we find that there is no significant change in the location of the center of mass of the Earth as a result of great earthquakes, and we do not consider any further this effect. However, there still remains the problem of the coseismic deformations changing the ITRF coordinates of sites on the surface of the Earth.

[32] We address this problem by using a "stable site" approach of carefully selecting sites in regions with modeled displacements of < 1 mm (see Figure 1) to define our reference frame. We assume that the coordinates of these sites are the same after the earthquake as before it. This then imposes the assumption that the origin has not moved. We then use this realization of the reference frame (which is essentially the "pre-earthquake" reference frame) to calculate changes in coordinates of sites in deformed areas. We selected three sites in Europe (Westerbroek, The Netherlands; Onsala, Sweden; Noto, Italy), two sites in

North America (St Johns, Canada; Flin Flon, Canada), two sites in Antarctica (Mawson and Davis) and one site in Australia (Yarragadee). Each of these sites has operated with minimal interruptions from 2000.0 to 2011.0, has a low amplitude of hydrological surface deformation [*Tregoning et al.*, 2009] and is present in over 95% of our daily GPS solutions.

[33] Our tests showed that the use of merely eight sites is sufficient to define a stable reference frame over the 2000–2011 period; indeed, including only one site per continent is sufficient to generate stable coordinate time series. We identified offsets in the time series of these eight sites (caused by equipment changes plus the coseismic deformation at Flin Flon during the Sumatra-Andaman earthquake) through constraining only four sites and then assessing the time series of the other four sites, then reversing the selection of reference sites. Once all offsets were removed from the time series of our reference sites, we were able to use all eight sites without fear of introducing biases into the coordinate estimates of the global network as a result of discontinuities in our reference frame definition.

[34] This approach generates time series of coordinate estimates that are less affected by the non-stationary variations of surface deformation at reference sites when substantially more reference sites are used. Of course, a bootstrapping process could be used to identify and correct for coseismic displacements at other sites; however, including more reference sites may introduce additional noise (caused by hydrological loading) and, for the purposes of this study, the use of only these eight sites provides a stable reference frame definition.

3.3. Offsets in Time Series

[35] The presence of Heaviside steps or offsets in time series is problematic when trying to estimate linear trends from observations. Our coordinate time series have a sufficiently low level of noise that we can estimate directly statistically significant offsets (sometimes as small as 0.5 mm) induced by instrument-related effects such as changes in antenna/receiver hardware and receiver firmware upgrades. Earthquake-related offsets can only be derived from individual time series because the deformation signals cancel out in differenced time series if the baselines are short, whereas instrument-related offsets can be derived either from individual coordinate time series or by differencing time series with nearby sites. We relied on the IGS site logs to provide accurate dates of changes in site hardware in addition to ITRF2008 discontinuities, and estimated offsets at these times. We used the "real sigma" approach described in *Reilinger et al.* [2006] to model realistically the noise of the GPS time series, then selected only estimated offsets that were different from zero at the 3σ level.

[36] For example, in Canberra, three IGS sites operate within 30 km: one at Tidbinbilla (TIDB) and two at Mt Stromlo (STR1, STR2). We identified a total of four instrument-related horizontal offsets at these sites—all $<$ 2.3 mm—through an assessment of differenced position time series. This approach yielded independent estimates that were found to be compatible at $<$ 0.2 mm. Importantly, the estimates derived from each individual time series alone differ by more than this level and we consider the "absolute" estimates to be less accurate, given the influence of time-correlated noise.

[37] We subsequently used the differenced time series approach to assess potential offsets at all sites on the Australian Plate and identified significant offsets at Yaragadee (YAR2), Ceduna (CEDU), Darwin (DARW) and Auckland (AUCK). This is the same approach that we used at each of our reference sites, generating differenced time series to nearby sites in order to estimate the equipment-induced offsets at the reference sites.

[38] The use of differenced time series from multiple sites colocated within several hundred meters provides a very accurate means of identifying submillimeter offsets introduced through instrument changes at any of the colocated sites (so long as firmware upgrades are not performed simultaneously at all sites). This provides strong support for the recommendations of the Global Geodetic Observing System that all key infrastructure sites in the global GPS network should have multiple sets of equipment observing simultaneously [*Rothacher et al.*, 2009].

3.4. Induced Velocity Errors

[39] What is the effect of small, uncorrected coseismic deformations on estimates of linear site velocities? We assessed this over the period of our analysis (2000.0–2011.0) by generating time series of modeled coseismic displacements at each GPS site in our global network as caused by the 15 great earthquakes. The trend of each time series then provides an estimate of the likely error that will be induced in velocity estimates if the far-field coseismic horizontal displacements are not accounted for (note that we are not considering here the interseismic strain accumulation that may occur at far-field sites; rather, simply the error in the linear trend estimates that the presence of coseismic discontinuities cause. The interseismic strain issue is likely to be a second-order effect and is not discussed in this study).

[40] We found that the horizontal velocity errors reach 0.2–0.4 mm/yr (Figure 1), even though the accumulated displacement from the great earthquakes amounts to only a few millimeters (of course, the magnitude of the error is a function of the time of the earthquake with respect to the time span of the GPS time series; however, we have generated these estimates using the actual timing of the great earthquakes over the past decade and so the errors are realistic). This level of error would degrade the accuracy of the terrestrial reference frame, potentially affecting the ability to estimate satellite orbits with sufficient accuracy to enable estimates of geophysical processes (e.g., sea level rise) with millimeter accuracy [*Beckley et al.*, 2007]. We show in section 4 that the errors can also affect continent-scale tectonic interpretations.

[41] Coseismic deformations exceeding $\sim$5 mm are often reported in the near- to medium-field [e.g., *Kreemer et al.*, 2006] and are accounted for in geophysical studies (i.e., sites located in the white regions of Figure 1); however, velocity errors will occur further afield as a result of the smaller, more distant coseismic deformations. Of particular note is the spatial coherence of the velocity errors in some regions, which would propagate into models of rigid plate rotations derived from GPS velocities estimated at the sites. Indeed, the velocity errors of nine sites in southern and central Africa

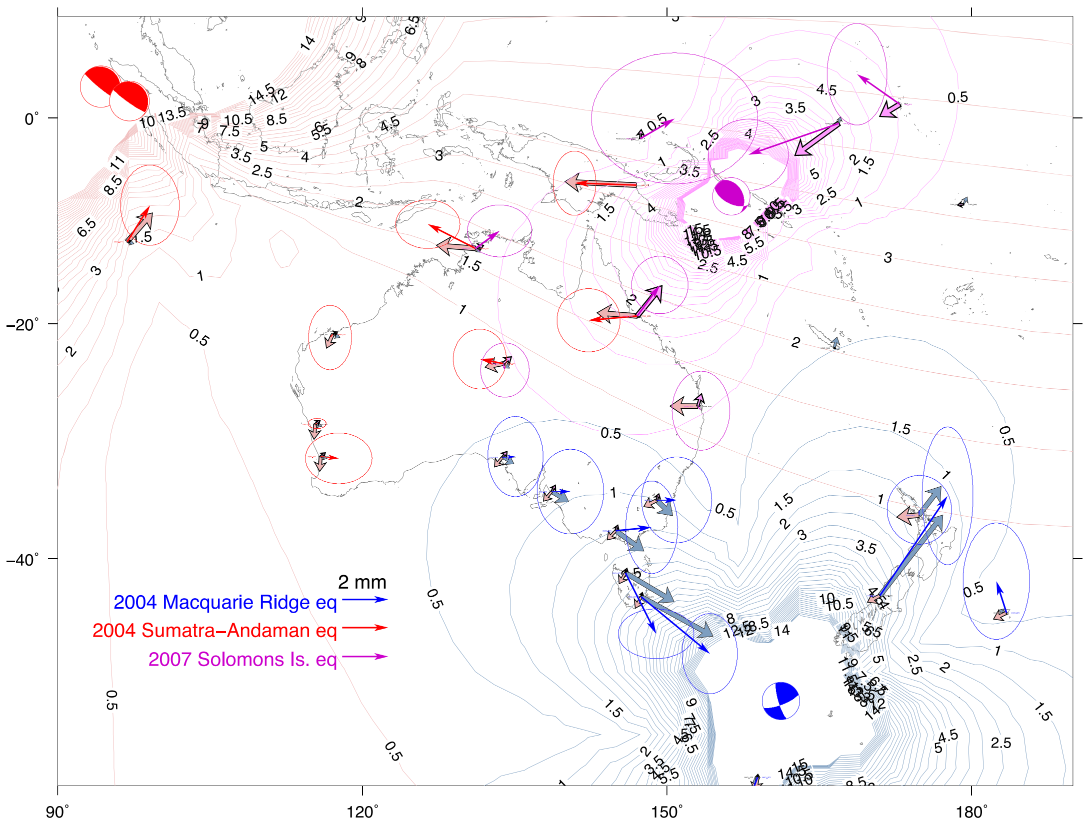

Figure 3. Coseismic horizontal displacements at GPS sites located on the Australian Plate. Focal mechanisms of the Sumatra-Andaman (red), Macquarie Island (blue) and Solomon Islands (pink) earthquakes were sourced from the Global Central Moment Catalogue. Contours of the magnitude of coseismic horizontal deformation for each earthquake are plotted along with the predicted horizontal displacements (thicker arrows, color-coded for each earthquake).

(see Figure 1) can be modeled by a single pole of rotation with an accuracy of ~0.02 mm/yr and induce a rotation error of ~0.02°/My into the definition of the Euler vector for the African Plate (around 7% of the actual plate rotation rate). Thus, far-field coseismic deformations will affect independent tectonic studies thousands of kilometers away from the earthquake rupture zones unless properly accounted for.

4. Case Study: Intraplate Deformation of the Australian Plate

[42] In this section, we undertake a typical tectonic study of the stability of a continental plate. We use this to demonstrate to what extent local tectonic studies can be affected by the horizontal deformations induced by far-field earthquakes and also to show how the selection of the strategy used to realize the coordinate reference frame can affect the tectonic interpretation.

[43] The amount of deformation of the Australian Plate from great earthquakes has been low this century when compared to other regions of the Earth. Australia is also one of the largest continental portions of a tectonic plate that does not have a diffuse plate boundary zone [*Gordon*, 1998] and is not experiencing rapid rates of horizontal motion due to present-day glacial isostatic adjustment (as is the case in, for example, North America and Europe). We therefore used GPS velocity estimates on this continent to assess to what extent a plate appears to be "rigid" over the first decade of the 21st Century. Nonetheless, before intraplate stability can be examined, we must first correct for small coseismic horizontal deformations that have occurred within the Australian Plate as a result of the distant great earthquakes: the 2007 Solomon Islands earthquake caused a significant (~1.7 mm) coseismic displacement at Townsville in northeast Australia, the 2004 Sumatra-Andaman earthquake displaced the GPS site at Darwin by 1.7 mm, while the Macquarie Ridge earthquake displaced Hobart (HOB2) by ~5 mm [*Watson et al.*, 2010]. No earthquake deformations were found to be statistically significantly different from zero at any other sites on mainland Australia.

[44] The modeled far-field deformations typically lie within the error ellipses of the GPS estimates of coseismic deformation (at the 95% confidence level). (Figure 3). This provides confidence in the far-field deformation modeling of the coseismic horizontal deformation field and also that the GPS offset estimates are detecting geophysical signal at the times of the earthquakes rather than just noise. While we did not rely on the earthquake models to correct our GPS time series for coseismic displacements (we estimated offsets directly from the time series themselves), this qualitative comparison demonstrates that the use of far-field GPS data is sensitive to these large-scale geophysical processes.

[45] We identify a small but consistent non-linear, postseismic relaxation deformation in the GPS time series of

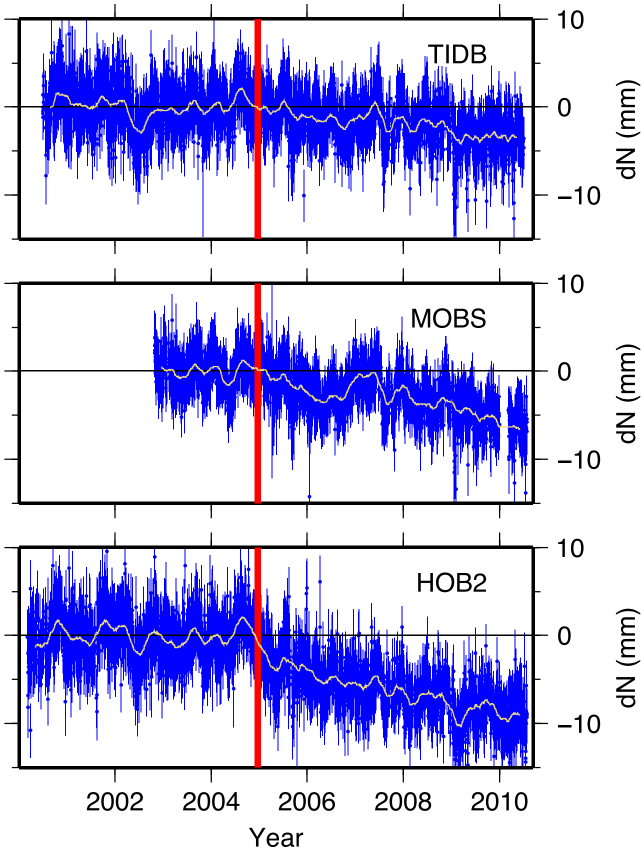

Figure 4. GPS time series of the north components at Hobart (HOB2), Melbourne (MOBS) and Canberra (TIDB), detrended over the pre-earthquake period (2000–2004.9). 100 day running mean is plotted. Vertical lines indicate the date of the Macquarie Island earthquake. Site locations are indicated on Figure 5.

sites along the eastern coast of Australia, decreasing with distance northward from the Macquarie Ridge earthquake epicenter. This is most prominent in the north component (Figure 4) and is actually of significantly greater magnitude than the coseismic deformation. Neither the coseismic deformation nor variations in the site velocity at Hobart, Melbourne or Canberra were identified in the most recent determination of the International Terrestrial Reference Frame *Altamini et al.* [2011]; therefore, the ITRF2008 does not account for this far-field earthquake deformation in southeastern Australia. This may explain some of the larger (i.e., > 0.4 mm/yr) residual velocities found by *Altamimi et al.* [2012] for sites on the Australian Plate. Because of the presence of ongoing post-seismic deformations at Hobart, Melbourne and Canberra (Figure 4), the velocities of these sites after the earthquake should no longer be represented by linear models.

[46] Once corrected for instrument offsets (see section 3.3), site velocities were estimated from the time series, with associated uncertainties derived using the "real sigma" approach [*Reilinger et al.*, 2006] to account for the non-Gaussian nature of GPS time series. Typical levels of uncertainties were ~0.3 mm/yr for sites with > 10 year data spans and ~1 mm/yr for sites with 2–5 year data spans. For the sites in southeastern Australia undergoing post-seismic deformation, we estimated a linear site velocity for only the time period before the 2004 Macquarie Ridge earthquake.

[47] Previous GPS studies have identified the Australian Plate as being a region of recent crustal stability, with internal deformation rates of < 2 mm/yr [*Tregoning*, 2003; *Sella et al.*, 2007; *Altamimi et al.*, 2012]. We inverted our site velocities to estimate a Euler vector to represent the rigid plate rotation of the Australian Plate. Several sites show significant horizontal motion with respect to the rigid plate motion: Perth (PERT) and Hillarys (HIL1) in southwestern WA and the southeastern GPS sites at HOB2, MOBS and TIDB. We attribute the motion of the first two sites to the extraction of groundwater [*Featherstone et al.*, 2012]. Indeed, the vertical velocities of these sites (not shown) identify subsidence of ~3 mm/yr over the past decade. The residual velocities of sites along the east coast of Australia may reflect interseismic strain accumulation prior to the 2004 Macquarie Ridge and 2007 Solomon Island

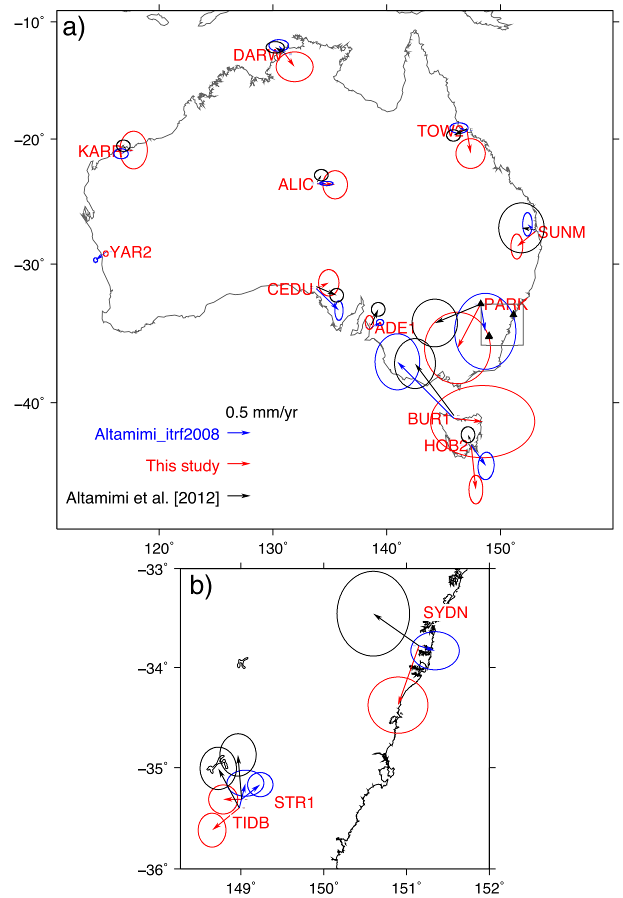

Figure 5. (a) Horizontal velocity residuals of GPS sites on the Australian Plate using our definition of the reference frame plus only six sites (YAR2, KARR, DARW, ALIC, CEDU, ADE1) to define the Australian Plate motion (red), and using the core IGS sites to define the reference frame plus the sites of *Altamimi et al.* [2012] to define the Australian Plate motion (blue). ITRF2008 residual velocities of *Altamimi et al.* [2012] are shown in black. (b) Zoom showing the velocity residuals at the sites in Canberra and Sydney.

earthquakes. We note that *Altamimi et al.* [2012] did not include HIL1, PERT or MOBS in the estimation of the rigid motion of the Australian Plate.

[48] After removing these five sites from the inversion, the remaining six sites show relative velocity vectors of < 0.2 mm/yr with respect to a rigid plate motion model for the Australian Plate (Figure 5). Our residual velocities at these sites have a root-mean-square (RMS) of 0.15 and 0.16 mm/yr for north and east, respectively—smaller than those of *Altamimi et al.* [2012] with a RMS of 0.17 and 0.21 mm/yr for north and east, respectively, for the velocity residuals of the same sites. This represents a reduction in RMS of around 11% and 23%.

[49] We interpret our value of 0.2 mm/yr to indicate an upper bound on the magnitude of current intraplate deformation across the Australian continent. However, it is clear that coseismic and post-seismic deformation is considerable even thousands of kilometers from the epicenters of the great earthquakes that have occurred around the fringe of the Australian Plate. The fact that coseismic deformation occurs implies that interseismic strain accumulation would have occurred prior to the earthquake ruptures, perhaps over decades to hundreds of years. Therefore, large tectonic plates should not be modeled as rigid bodies, and models of tectonic motion implicit in the definition of the terrestrial reference frame need to be more complex than simply representing continental drift with a linear velocity.

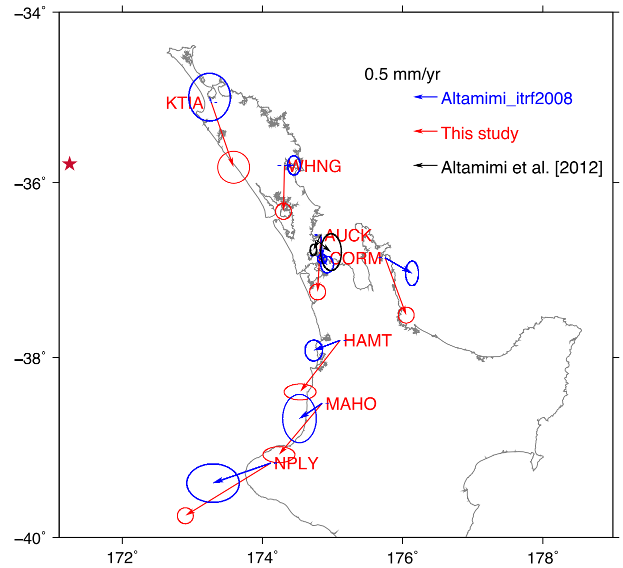

Figure 6. Same as in Figure 5, but showing the residual velocities for sites in the North Island of New Zealand. The relative pole of rotation that fits these vectors is indicated with a star.

4.1. New Zealand

[50] We now apply our plate model and GPS analysis to address the question of whether the North Island of New Zealand moves as part of the rigid Australian Plate, as it has been suggested or assumed by several studies [e.g., *Tregoning*, 2002, 2003; *Wallace et al.*, 2004; *Sella et al.*, 2007; *Altamimi et al.*, 2012] that Auckland (AUCK) (see Figure 6) lies on the Australian Plate. Note that motion of sites in the central and eastern regions of the North Island regularly experience non-linear motion as a result of slow slip events on the Hikurangi Trench [e.g., *Wallace et al.*, 2004; *Wallace and Beavan*, 2006], and we do not attempt to estimate residual linear velocities in this region.

[51] Our analysis of a network of sites along the west coast of the North Island of New Zealand shows significant motion relative to our model of the rigid Australian Plate (Figure 6). The pattern of relative velocities can be modeled as a rigid block rotation of ∼0.28±0.03°/My about an Euler pole located at S35.78°, E171.25°. This would be consistent with possible transform motion on the van der Linden Fault and the Vening Meinesz Fracture Zone north of the North Island [*Sutherland*, 1999]. Alternatively, the deformation could indicate interseismic strain accumulation associated with the Australia-Pacific Plate boundary that will be released by the next great earthquake or slow slip event in the region. In either case, none of the sites spanning the North Island of New Zealand should be considered to be moving as part of the rigid Australian Plate.

4.2. Tectonic Interpretation From an Alternate Coordinate Reference Frame Definition

[52] To demonstrate how the definition of the terrestrial reference frame influences the horizontal velocities derived from the time series of GPS coordinates, we generated a second set of site velocities from our daily GPS solutions, this time using a different set of sites and discontinuities to define the reference frame. For this second solution, we used ∼30–40 of the core IGS sites [*Rebischung et al.*, 2012] and the associated set of offsets that comprise the IGS2008. This includes several sites on the Australian Plate and some of the sites for which our solutions show non-linear motion (e.g., HOB2, TIDB). The time series generated in this manner typically has a higher level of noise, which we attribute to the hydrological loading and possible discontinuities/non-linear motions at the additional core sites propagating through the transformation into the coordinates of other sites.

[53] We generated an estimate of the Euler vector for the Australian Plate using the same set of sites to define the plate motion as was used in ITRF2008 [*Altamimi et al.*, 2012], then computed residual velocity vectors with respect to this definition of the plate motion (blue vectors in Figure 5). Of the 14 sites on the Australian continent, only three of the error ellipses (95% confidence level) of the residual horizontal velocities overlap between our preferred solution and that of the second solution (using the ITRF2008 core sites to stabilize the reference frame plus the enlarged selection of sites to define the Australian Plate motion). In some cases, the residuals are considerably larger than those of our preferred solution. For example, convergence of ∼0.7±0.14 mm/yr (1σ) is implied between Ceduna and Adelaide, whereas our preferred solution shows –0.2±0.2 mm/yr (1σ uncertainties). Additionally, the relative residual vectors at Burnie and Hobart, Tasmania, suggest extension of ∼2.2±0.3 mm/yr across Tasmania and convergence of ∼2.2±0.3 mm/yr between Tasmania and Adelaide. There is no tectonic evidence for any of these motions. Furthermore, all of these sites have been used to define the rigid motion of the Australian Plate so, by construction, one would not expect to find relative motion between the sites.

[54] Not accounting for non-linear deformation signals caused by distant great earthquakes degrades the accuracy of linear velocity estimates. Our horizontal velocity estimate for Hobart using only data prior to the 2004 Macquarie Ridge earthquake is 56.15±0.07 and 14.03±0.06 mm/yr for the north and east components, respectively (north component is shown in Figure 4), compared to 55.67±0.12 and 14.34±0.08 mm/yr when fitting a linear trend through all the observations, including the post-seismic period (we applied the ITRF2008 offset to correct for the coseismic displacement at HOB2, but make no correction for the post-seismic relaxation since this is not accounted for in ITRF2008). Velocity errors of ~0.3 and ~0.05 mm/yr also occur at MOBS and TIDB, respectively, showing a decrease in error further away from the earthquake epicenter. Thus, failing to account for far-field post-seismic deformation can introduce velocity errors as large as 0.5 mm/yr, larger than the uncertainties of the velocity estimates and significantly larger than the level of rigidity of the western part of the Australian Plate.

[55] Additionally, we estimated residual velocity vectors for the sites in the North Island of New Zealand with respect to this second definition of the motion of the Australian Plate (blue arrows in Figure 6). The rotation of the western North Island w.r.t. the Australian Plate that is seen in the residual velocities of our preferred solution is no longer evident, with the sites north of ~S37° showing insignificant motion relative to the Australian Plate—probably caused by the inclusion of the velocities of two sites in Auckland into the definition of the Australian Plate motion. In this latter solution, right-lateral strike slip motion is required between Auckland and Hamilton, whereas in our preferred, the residual velocities can be explained by a block rotation of the entire region relative to the Australian Plate. Thus, the more general selection of key sites from which to define the terrestrial reference frame and the rigid Australian Plate leads to less clarity in the interpretation of the residual velocities, and requires small crustal deformations between certain sites when there is no evidence for such tectonic activity.

5. Conclusions

[56] Earthquakes account for much of the deformation of the Earth's surface, and large earthquakes will continue to cause measurable step offsets in geodetic position time series. Between one and 20 earthquakes of $M_w > 8$ occur each decade, deforming around 50% of the surface of the Earth with amplitudes > 1 mm. Areas along particular nodal lines of the great earthquakes, at the extensions of the strikes of the fault ruptures, experience the smallest amounts of deformation. Thus, defining and maintaining a stable terrestrial reference frame over multiple decades to support studies of the dynamic Earth system is extremely problematic because, at unknown and irregular intervals, virtually the entire tracking network will move abruptly in an unpredictable manner. We have shown that this deformation can induce linear velocity errors of up to 0.4 mm/yr at sites over 1000 km from the earthquake locations.

[57] However, it is possible to mitigate the consequences of these problems and thus generate secular motion estimates with accuracies of 0.2 mm/yr or better through the careful selection of reference sites in nodal areas of least coseismic deformation. Thus, through an adaptive process, earthquake deformations at other sites could then be corrected, resulting in a long-term, stable reference frame. With a careful selection of sites to define the terrestrial reference frame, sub-millimeter accuracy of site velocities is possible over decadal time scales at the level claimed for the most recent International Terrestrial Reference Frame [*Altamimi et al.*, 2012], but it is important that changes in instrument hardware that cause coordinate offsets are first detected and removed with the highest accuracy possible.

[58] Despite the occurrence of a high number of great earthquakes, including three on its plate boundaries, a large portion of the Australian Plate (excluding the SE regions of Tasmania, Victoria and parts of New South Wales) is deforming at < 0.2 mm/yr, making it one of the most stable crustal regions in the world. However, motion of GPS sites located even thousands of kilometers from active interplate boundaries can still be contaminated by earthquake deformations. The improved resolution of our GPS analysis permitted the identification of nonlinear post-seismic relaxation along the east coast of Australia, as noted previously by *Watson et al.* [2010]. We note that this post-seismic deformation is not considered in ITRF2008 [*Altamimi et al.*, 2011, 2012] but amounts to ~5–10 mm in the 5 years following the Macquarie Ridge earthquake.

[59] While small in magnitude, both earthquake and instrument effects must first be accounted for in order to be able to identify the true level of intraplate rigidity and to recognize local deviations from it. Careful selection of sites located on the "rigid" part of tectonic plates is also important; otherwise, incorrect interpretations of the residual deformation fields can occur as demonstrated for the case of southeast Australia and the North Island of New Zealand. The detection of small-magnitude crustal deformations can only be drawn from state-of-the-art GPS analysis and modelling, accounting first for time varying atmospheric effects, atmospheric pressure loading deformation, coseismic earthquake deformation of distant earthquakes and instrument offset identification.

[60] **Acknowledgments.** This research was supported under the Australian Research Council's Discovery Projects funding scheme (DP0877381). We thank the IGS for making global GPS data freely available and Frank Pollitz for sharing his spherical earthquake deformation code. Figures were plotted using GMT [*Wessell and Smith*, 1998]. Part of this work was conducted while S.L. was on sabbatical at ANU. The GPS data were computed on the Terrawulf II computational facility at the Research School of Earth Sciences, a facility supported through the AuScope initiative. AuScope Ltd is funded under the National Collaborative Research Infrastructure Strategy NCRIS), an Australian Commonwealth Government Programme. We thank the Associate Editor and two anonymous reviewers for review comments.

References

Altamimi, Z., X. Collilieux, and L. Métivier (2011), ITRF2008: An improved solution of the International Terrestrial Reference Frame, *J. Geod.*, *85*, 457–473, doi:10.1007/s00190-011-0444-4.

Altamimi, Z., L. Métivier, and X. Collilieux (2012), ITRF2008 plate motion model, *J. Geophys. Res.*, *117*, B07402, doi:10.1029/2011JB008930.

Banerjee, P., F. Pollitz, B. Nagarajan, and R. Bürgmann (2007), Coseismic slip distributions of the 26 December 2004 Sumatra-Andaman and 28 March 2005 Nias earthquakes from GPS static offsets, *Bull. Seis. Soc. Am.*, *97*, S86–S102.

Beavan, J., X. Wang, C. Holden, K. Wilson, W. Power, G. Prasetya, M. Bevis, and R. Kautoke (2010), Near-simultaneous great earthquakes at Tongan megathrust and outer rise in September 2009, *Nature*, *466*(7309), 959–U978.

Beckley, B. D., F. G. Lemoine, S. B. Luthcke, R. D. Ray, and N. P. Zelensky (2007), A reassessment of global and regional mean sea level trends from TOPEX and Jason-1 altimetry based on revised reference frame and orbits, *Geophys. Res. Lett.*, *34*, L14608, doi:10.1029/2007GL030002.

Boehm, J., B. Werl, and H. Schuh (2006), Troposphere mapping functions for GPS and very long baseline interferometry from European Centre for Medium-Range Weather Forecasts operational analysis data, *J. Geophys. Res.*, *111*, B02406, doi:10.1029/2005JB003629.

Chao, B. F., and R. S. Gross (1987), Changes in the Earths rotation and low-degree gravitational eld induced by earthquakes, *Geophys. J. Royal Astr. Soc.*, *91*, 569–596.

Dziewonski, A. M., and D. L. Anderson (1981), Preliminary reference Earth model, *Phys. Earth Planet. Int.*, *25*, 297–356.

Ekström, G., M. Nettles, and A. M. Dziewoński (2012), The global CMT project 20042010: Centroid-moment tensors for 13,017 earthquakes, *Phys. Earth Planet. Int.*, *200201*, 1–9, doi:10.1016/j.pepi.2012.04.002.

Featherstone, W. E., M. S. Filmer, N. T. Penna, L. M. Morgan, and A. Schenk (2012), Anthropogenic land subsidence in the Perth Basin: Challenges for its retrospective geodetic detection, *J. Royal Soc. Western Aust.*, *95*, 53–62.

Fu, G., and W. Sun (2006), Global co-seismic displacements caused by the 2004 Sumatra-Andaman earthquake (Mw 9.1), *Earth, Planets, Space*, *58*, 149–152.

Furlong, K. P, T. Lay, and C. J. Ammon (2009), A great earthquake rupture across a rapidly evolving three-plate boundary, *Science*, *324*, 226–229.

Gordon, R. G. (1998), The plate tectonic approximation: Plate nonrigidity, diffuse plate boundaries, and global plate reconstructions, *Annu. Rev. Earth Planet. Sci.*, *26*, 615–642.

Gross, R. S., and B. F. Chao (2006), The rotational and gravitational signature of the December 26, 2004 Sumatran earthquake, *Surv. Geophys.*, *27*, 615–632.

Herring, T. A., R. W. King, and S. C. McClusky (2010), GAMIT reference manual, release 10.4: *Cambridge, Massachusetts Institute of Technology Department of Earth, Atmospheric, and Planetary Sciences,* 171 pp.

Konca, A. O., et al. (2008), Partial rupture of a locked patch of the Sumatra megathrust during the 2007 earthquake sequence, *Nature*, *456* (7222), 631–635.

Kreemer, C., G. Blewitt, W. C. Hammond, and H-P Plag (2006), Global deformation from the great 2004 Sumatra-Andaman Earthquake observed by GPS: Implications for rupture process and global reference frame, *Earth, Planets, Space*, *58*, 141–148.

Lay, T., H. Kanamori, C. J. Ammon, A. R. Hutko, K. Furlong, and L. Rivera (2009), The 20062007 Kuril Islands great earthquake sequence, *J. Geophys. Res.*, *114*, B11308, doi:10.1029/2008JB006280.

Lay, T., C. J. Ammon, H. Kanamori, L. Rivera, K. D. Koper, and A. R. Hutko (2010), The 2009 Samoa-Tonga great earthquake triggered doublet, *Nature*, *466*(7309), 964–U985.

Lorito, S., F. Romano, S. Atzori, X. Tong, A. Avallone, J. McCloskey, M. Cocco, E. Boschi, and A. Piatanesi (2011), Limited overlap between the seismic gap and coseismic slip of the great 2010 Chile earthquake, *Nat. Geosci.*, *4*(3), 173–177.

Park, S.-C., and J. Mori (2007), Triggering of earthquakes during the 2000 Papua New Guinea earthquake sequence, *J. Geophys. Res.*, *112*, B03302, doi:10.1029/2006JB004480.

Pollitz, F. F. (1996), Coseismic deformation from earthquake faulting on a layered spherical earth, *Geophys. J. Int.*, *125*, 1–14.

Pritchard, M. E., E. O. Norabuena, C. Ji, R. Boroschek, D. Comte, M. Simons, T. H. Dixon, and P. A. Rosen (2007), Geodetic, teleseismic, and strong motion constraints on slip from recent southern Peru subduction zone earthquakes, *J. Geophys. Res.*, *112*, B03307, doi:10.1029/2006JB004294.

Ray, J., Z. Altamimi, X. Collieux, and T. van Dam (2008), Anomalous harmonics in the spectra of GPS position estimates, *GPS Solutions*, *12*, 55–64, doi:10.1007/s10291-007-0067-7.

Rebischung, P., J. Griffiths, J. Ray, R. Schmid, X. Collilieux, and B. Garay (2012), IGS08: the IGS realization of ITRF2008, *GPS Solutions*, *16*, 483–494, doi:10.1007/s10291-011-0248-2.

Reilinger, R., et al. (2006), GPS constraints on continental deformation in the Africa-Arabia-Eurasia continental collision zone and implications for the dynamics of plate interactions, *J. Geophys. Res.*, *111*, B05411, doi:10.1029/2005JB004051.

Rothacher, M., et al. (2009), The future global geodetic observing system, in *Global Geodetic Observing System: Meeting the Requirements of a Global Society on a Changing Planet in 2020*, edited by H.-P. Plag, and M. Pearlman, pp. 237–270 , Springer, Berlin, Heidelberg.

Romano, F., A. Piatanesi, S. Lorito, and K. Hirata (2010), Slip distribution of the 2003 Tokachi-oki Mw 8.1 earthquake from joint inversion of tsunami waveforms and geodetic data, *J. Geophys. Res.*, *115*, B11313, doi:10.1029/2009JB006665.

Sella, G. F., S. Stein, T. H. Dixon, M. Craymer, T. S. James, S. Mazzotti, and R. K. Dokka (2007), Observation of glacial isostatic adjustment in "stable" North America with GPS, *Geophys. Res. Lett.*, *34*, L02306, doi:10.1029/2006GL0270812.

Simons, M., et al. (2011), The 2011 magnitude 9.0 Tohoku-Oki earthquake: Mosaicking the megathrust from seconds to centuries, *Science*, *332*(6036), 1421–1425.

Sladen, A., H. Tavera, M. Simons, J. P. Avouac, A. O. Konca, H. Perfettini, L. Audin, E. J. Fielding, F. Ortega, and R. Cavagnoud (2010), Source model of the 2007 Mw 8.0 Pisco, Peru earthquake: Implications for seismogenic behavior of subduction megathrusts, *J. Geophys. Res.*, *115*, B02405, doi:10.1029/2009JB006429.

Steigenberger, P., J. Boehm, and P. Tesmer (2009), Comparison of GMF/GPT with VMF1/ECMWF and implications for atmospheric loading, *J. Geod.*, *83*, 943–951.

Sutherland, R. (1999), Basement geology and tectonic development of the greater New Zealand region: An interpretation from regional magnetic data, *Tectonophys.*, *308*, 341–362.

Tang, L., V. V. Titov, Y. Wei, H. O. Mofjeld, M. Spillane, D. Arcas, E. N. Bernard, C. Chamberlin, E. Gica, and J. Newman (2008), Tsunami forecast analysis for the May 2006 Tonga tsunami, *J. Geophys. Res.*, *113*, C12015, doi:10.1029/2008JC004922.

Tregoning, P. (2002), Plate kinematics in the western Pacific derived from GPS observations, *J. Geophys. Res.*, *107*, doi:10.1029/JB2001000406.

Tregoning, P. (2003), Is the Australian Plate deforming? A space geodetic perspective, Geol, *Soc. Aus. Special Publication, 22,* and *Geol. Soc. Am. Special Publication*, *372*, 41–48.

Tregoning, P., and C. Watson (2009), Atmospheric effects and spurious signals in GPS analyses, *J. Geophys. Res.*, *114*, B09403, doi:10.1029/2009JB006344.

Tregoning, P., and C. Watson (2011), Correction to"Atmospheric effects and spurious signals in GPS analyses," *J. Geophys. Res.*, *116*, B02412, doi:10.1029/2010JB008157.

Tregoning, P., C. Watson, G. Ramillien, H. McQueen, and J. Zhang (2009), Detecting hydrologic deformation using GRACE and GPS, *Geophys. Res. Lett.*, *36*, L15401, doi:10.1029/2009GL038718.

Vigny, C., et al. (2005), Insight into the 2004 Sumatra-Andaman earthquake from GPS measurements in Southeast Asia, *Nature*, *436*, 201–206.

Wallace, L. M., J. Beavan, R. McCaffrey, and D. Darby (2004), Subduction zone coupling and tectonic block rotations in the North Island, New Zealand, *J. Geophys. Res.*, *109*, B12406, doi:10.1029/2004JB003241.

Wallace, L. M., and J. Beavan (2006), A large slow slip event on the central Hikurangi subduction interface beneath the Manawatu region, North Island, New Zealand, *Geophys. Res. Lett.*, *33*, L11301, doi:10.1029/2006GL026009.

Watson, C. S., R. Burgette, P. Tregoning, N. White, J. Hunter, R. Coleman, R. Handsworth, and H. Brolsma (2010), Twentieth century constraints on sea level change and earthquake deformation at Macquarie Island, *Geophys. J. Int.*, *182*, 781–796, doi:10.1111/j.1365-246X.2010.04640.X.

Wessell, P., and W. H. F. Smith (1998), New, improved version of generic mapping tools released, *EOS Trans. AGU*, *79*(47), 579.

Williams, S., and N. Penna (2011), Non-tidal ocean loading effects on geodetic GPS heights, *Geophys. Res. Lett.*, *38*, L09314, doi:10.1029/2011GL046940.

Yagi, Y., and Y. Fukahata (2011), Rupture process of the 2011 Tohoku-oki earthquake and absolute elastic strain release, *Geophys. Res. Lett.*, *38*, L19307, doi:10.1029/2011GL048701.